nature communications

Article

https://doi.org/10.1038/s41467-025-62480-9

Kerr non-linearity enhances the response of a graphene Josephson bolometer

Received: 7 February 2025

Accepted: 22 July 2025

Joydip Sarkar[1], Krishnendu Maji[1], Abhishek Sunamudi[1,2], Heena Agarwal[1], Priyanka Samanta[1], Anirban Bhattacharjee[1], Rishiraj Rajkhowa[1], Meghan P. Patankar[1], Kenji Watanabe[3], Takashi Taniguchi[4] & Mandar M. Deshmukh[1]

Bolometers are radiation sensors that are central to wide areas such as dark matter search, radio astronomy, material science, and qubit readouts, among others. There have been different kinds of bolometer realizations in the recent past. The challenge is to have a single device that combines high sensitivity, broad bandwidth, and a fast readout scheme. Here we demonstrate the usage of Josephson parametric amplifiers (JPA) as highly sensitive bolometers. Our key finding is that the Kerr non-linearity of the JPA boosts the device's sensitivity. When the bolometer is biased in the non-linear regime, it enhances the up-converted signals (~100 times), resulting in an order of magnitude improvement in sensitivity compared to the linear regime. In the non-linear biasing, we achieve a NEP ~ 500 $\mathrm{aW}/\sqrt{\mathrm{Hz}}$. Our device offers a fast detection scheme with a thermal time constant of 4.26 μs and an intrinsic JPA time constant of 70 ns. Our work integrates a JPA into a bolometer, enabling a fast and sensitive operation compared to previously studied graphene-based bolometers. Our study demonstrates a way forward to improve the quantum sensors based on 2D materials by leveraging the inherent non-linear response.

Sensing single photons in the radio frequency (RF) range is challenging because of the low photon energies compared to THz or near-infrared (NIR). However, sensitive bolometers in the radio frequency range are at the heart of radio astronomy and dark matter search experiments[1,2]. There are various types of bolometers utilizing different physical platforms, such as transition edge sensor (TES)[3], microwave kinetic inductance detector (MKID)[4], quantum dot-based[5], superconducting qubit-based[6,7], graphene-based[8,9], graphene Josephson junction (JJ)-based[10–12], and superconducting nanowire-based (SNSPD)[13] sensors among others. The key performance metrics of any bolometer include noise equivalent power (NEP), response time (τ), instantaneous frequency bandwidth, and operational frequency range. However, achieving optimal performance across all these metrics in a single device is challenging. Currently, the best NEP for microwave photons is $10^{-22}\ \mathrm{W}/\sqrt{\mathrm{Hz}}$ using a superconducting qubit-based bolometer[7]. However, this device operates within a narrow bandwidth of ~50 MHz and requires a long integration time. Whereas, the fastest graphene-based bolometer operates with a very short thermal relaxation time of 35 ps[9]. Nonetheless, its NEP is relatively modest at $10^{-12}\ \mathrm{W}/\sqrt{\mathrm{Hz}}$. Therefore, efforts are required to improve all these aspects at a single-device level.

Over the past decade, single-photon bolometers based on graphene have gained popularity because of their high performance across a broad electromagnetic spectrum and their rapid response times. Graphene has many attractive electrical and thermal properties, rendering it a promising material for bolometry and calorimetry. At the charge neutrality, graphene has a vanishing density of states, resulting in small heat capacity and electron-to-phonon thermal coupling, which are highly desirable properties for bolometers[8]. It has been shown that

---

[1]Department of Condensed Matter Physics and Materials Science, Tata Institute of Fundamental Research, Mumbai, India. [2]Indian Institute of Science Education and Research Kolkata, Mohanpur, West Bengal, India. [3]Research Center for Functional Materials, National Institute for Materials Science, Tsukuba, Japan. [4]International Center for Materials Nanoarchitectonics, National Institute for Materials Science, Tsukuba, Japan.
e-mail: joydips581@gmail.com; deshmukh@tifr.res.in

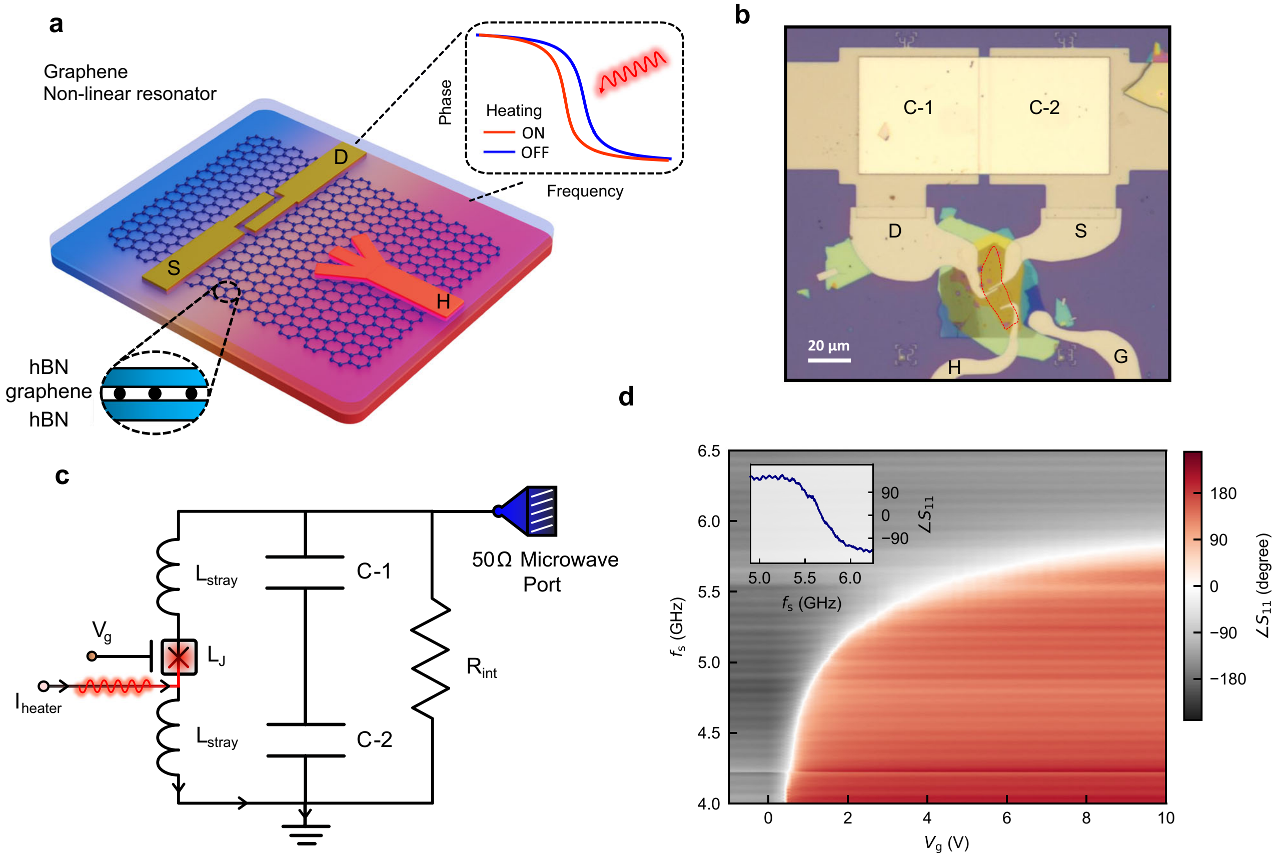

Fig. 1 | Device image, circuit model, and microwave response of the device. **a** Shows the schematic of our bolometer device, the Josephson junction (JJ) is made on an hBN-graphene-hBN stack, where hBN stands for hexagonal boron nitride. We implement a separate heater line inside the device to inject the heating signals. In the image, S, D, and H imply the source, drain, and heater electrodes, respectively. The inset figure in the dashed box illustrates the working scheme of our device based on the resonance frequency shift upon heating. The individual traces indicate the phase change at resonance. **b** Shows a zoomed optical micrograph of our Josephson parametric amplifier (JPA) bolometer device. The graphene JJ is in parallel to a series combination of two parallel plate capacitors C-1 and C-2 having identical dimensions of 60 × 60 µm². The red dashed line indicates the position of the sandwiched graphene flake. In the image, S, D, G, and H indicate the source, drain, gate, and heater electrodes, respectively. The heater line connects to the edge of the extended graphene flake, which is substantially away from the junction. When the heater current flows, it causes Joule heating in the extended graphene flake shared with the JJ; in turn, the generated heat propagates and increases the local temperature of the junction. The heater current drains to the ground plane of the coplanar waveguide. **c** Shows the equivalent lumped element circuit model of the device, where L_J is the junction inductance, L_{stray} is the stray inductance, C-1 and C-2 are the two parallel plate capacitors in series, R_{int} is to account for internal losses in the device, I_{heater} is the heater current, and V_g is the applied gate voltage to the JJ. The heater current is sent from a heater port and drains to the ground. The device is connected to a microwave port through a 50 Ω matched environment for reflection-based measurements. **d** Shows reflected phase ($\angle S_{11}$) of the device plotted as a function of signal frequency (f_s) and applied gate voltage (V_g). The linear resonance frequency of the device ($f_{\text{res}}^{\text{lin}}$) gets tuned as a function of gating. The gate voltage tunes the linear resonance in a large frequency band of 4–5.7 GHz. The 2π phase change at resonance indicates that the device is over coupled ($Q_{\text{int}} \gg Q_{\text{ext}}$) all along the electron doping side. The inset shows a line slice of the phase plot at $V_g = 6$ V.

graphene efficiently absorbs photons across a wide frequency spectrum starting from GHz to NIR[9,14,15]. The short electron-electron scattering time in graphene facilitates rapid equilibration of energy from absorbed photons[16,17]. Recently, superconductor-normal-superconductor (SNS) Josephson junctions have been used for bolometry harnessing the sensitivity of JJs[10–12,18–20]. While these experiments have demonstrated highly sensitive operations, some utilize a low-frequency switching scheme to operate the device, which limits the bolometer's response time. Additionally, all these experiments show very narrow bandwidth operation and none of them have exploited the non-linear response of a JJ for sensing. Hence, there is scope for improving the sensitivity, response time, and bandwidth of these devices, and we focus on these aspects in our work.

To devise a highly sensitive and fast bolometer, we employ a graphene-based JPA architecture. JPAs are widely used for quantum sensing and readout purposes in circuit quantum electrodynamics (cQED) experiments[21]. Because of the high sensitivity of the JPA nonlinearity and quantum noise-limited operation, such devices have the potential to sense at individual photon levels with minimal backaction[22–24]. While the previous realizations of graphene-based bolometers have exploited the temperature-dependent resistance, inductance, or switching events in JJs, the temperature-dependent non-linear Josephson inductance has been unexplored. In this work, we demonstrate a graphene JPA as a highly sensitive bolometer. We implement a separate heater line inside the device to inject RF signals onto the graphene flake. We measure the heater-modulated sideband response of the bolometer and extract the NEP and response time of the device experimentally.

Results

Device description

Figure 1 a–c shows the schematic, optical image, and circuit model of the bolometer device. The device contains a superconducting coplanar waveguide (CPW) where the central line is terminated to the ground through a lumped element LC resonator made from a parallel plate capacitor and a graphene JJ, which serves as an inductor. The device is designed to have a low-quality factor (~10) using a directly coupled architecture that helps in fast readout from the device. The JJ

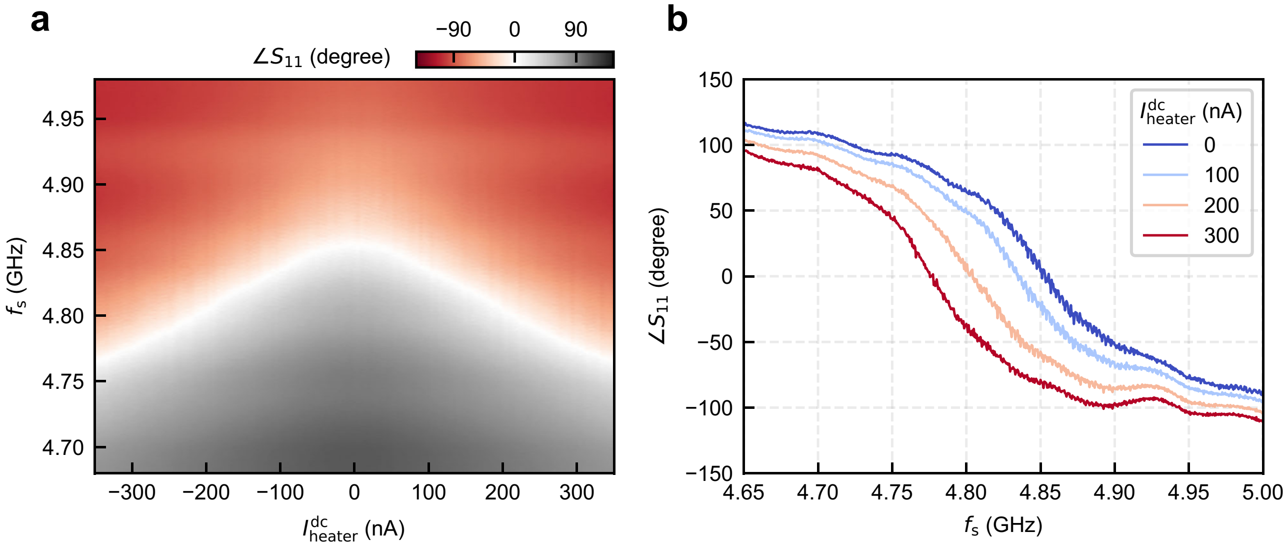

Fig. 2 | Resonance frequency shift of the bolometer due to heating. a Shows the low-power reflected phase ($\angle S_{11}$) of the device as a function of dc heater current ($I^{\mathrm{dc}}_{\mathrm{heater}}$) and microwave signal frequency (f_s) at $V_g = 1$ V. The white color in the plot indicates the decreasing resonant feature of the device. The Joule heating caused by the heater current reduces the switching current (I_c) and increases the Josephson inductance of the junction. The decrease in the linear resonance frequency with heating is consistent with the $f^{\mathrm{lin}}_{\mathrm{res}} \propto \sqrt{I_c}$ prediction. **b** Shows the line slice of the color plot in (**a**) for different values of the DC heater currents ($I^{\mathrm{dc}}_{\mathrm{heater}}$).

is made on an hBN-graphene-hBN stack. We make a separate electrode close to the JJ (~10 µm away) to inject heating signals onto the graphene flake. The graphene JJ and heater are on the same sheet of graphene that also serves as the bus for carrying excitations.

The essential idea here is that for a JPA, the reflected signal's phase is a very sensitive parameter due to its nonlinear nature. Consequently, any minute heating effect causes a resonance frequency or phase shift in the device. The current-phase relation (CPR) of the graphene JJ, including the first non-linear term, can be written as $I_s(\phi) \cong (\alpha\phi + \beta\phi^3)$, for a small ϕ approximation around zero. Where, I_s is the supercurrent, ϕ is the phase difference across the junction, α and β are the expansion coefficients. The Josephson inductance is given by $L_J(\phi) = \frac{\hbar}{2e}\left(\frac{\partial I_s}{\partial \phi}\right)^{-1}$, where $\hbar$ is the reduced Planck's constant and e is the electronic charge. Hence, the non-linear inductance can be approximated as $L_J(\phi) \cong L_0 + L_2\phi^2$, where L_0 and L_2 are the nonlinear inductor coefficients. This cubic nonlinearity in the CPR, known as the Kerr term, gives rise to a nonlinear junction inductance that is essential for parametric amplification. In our JPA bolometer device, we explore the effect of heating and the consequent phase shift in the device. When the heater signal is modulated, the resulting phase shift generates frequency up-converted sideband signals, which we use as markers for sensing.

Device characterization

We begin with a basic microwave characterization of the device and then move to the bolometer measurements. We probe the device with low-power microwave signals and measure the reflected signals using a vector network analyzer (VNA). For DC characterization of the device, see Supplementary Note 1. The measurements were done in a dilution fridge at 20 mK temperature (see Supplementary Note 2 for details on the setup). We check the gate tunability of the JPA and observe broad tunable resonance over a band of ~2 GHz, see Fig. 1d. Next, we proceed to do bolometer characterization, where we measure the reflected phase ($\angle S_{11}$) of the device as a function of signal frequency (f_s) and applied dc heater current ($I^{\mathrm{dc}}_{\mathrm{heater}}$) at a fixed gate voltage ($V_g = 1$ V), see Fig. 2a. The Joule heating caused by the heater current reduces the switching current (I_c) and increases the Josephson inductance of the junction. We observe a decrease in the linear resonance frequency with heating, consistent with the $f^{\mathrm{lin}}_{\mathrm{res}} \propto \sqrt{I_c}$ prediction. This holds when the stray inductance is minimized compared to the Josephson inductance. In our devices the Josephson inductance is at least 3 times larger than the stray inductance contribution of the JJ arms. We see a large tunability of the resonance frequency with the gate voltage without saturation even at high V_g, as the Josephson inductance dominates over the stray inductance. In Fig. 2b, we show the line slice of Fig. 2a at different heater currents.

Modulated heating experiments

Next, to extract the sensitivity of the bolometer, we perform the heater modulation experiments. In Fig. 3a, we explain the frequency conversion and sideband generation scheme due to modulated heating. A modulated heater signal causes the JPA phase ($\angle S_{11}$) at a certain frequency to oscillate over time, resulting in the generation of sidebands in the frequency domain. The Joule heating effect of any modulated current at frequency f_h produces sidebands at $f_s \pm 2f_h$, where f_s is the pump signal frequency, set near the resonance. See Supplementary Note 12 for a theoretical description of the observed sideband features. Fig. 3b shows the experimental sideband data from the device measured using a spectrum analyzer, we send a heater signal at a frequency f_h = 1 MHz and heater power $P_{\mathrm{heater}} = -78$ dBm. We see the up-converted sideband signals at twice the frequencies ($2f_h$ = 2 MHz) along with the pump signal in the middle. The pump signal is set near the non-linear regime of the bolometer with f_s = 5.47 GHz, $P_s = -79.77$ dBm, and $V_g = 6$ V. The on-flake heating scheme in our device works from DC to 100 MHz heater signal frequencies; see Supplementary Note 7 for sideband data at different heater frequencies and Supplementary Note 8 for different gate voltages. Now, to check the heater sensitivity, in Fig. 3c we plot the right sideband (RSB) signal power measured as a function of the detuned frequency (δf) and heater power. As we increase the heater power the sideband signal rises and eventually saturates, indicating saturation of the bolometer.

We quantify the sensitivity of our device through the sideband measurements as discussed in Fig. 3c. We have observed that when the bolometer is biased in the non-linear regime, it is very sensitive to heater modulations. Fig. 3d shows a non-linear phase diagram of the bolometer, where we measure the reflected phase ($\angle S_{11}$) of the device as a function of microwave signal frequency (f_s) and power (P_s). This is the typical non-linear phase diagram of a JPA with a cubic non-linear term in the CPR. See Supplementary Note 14 for a calculated phase

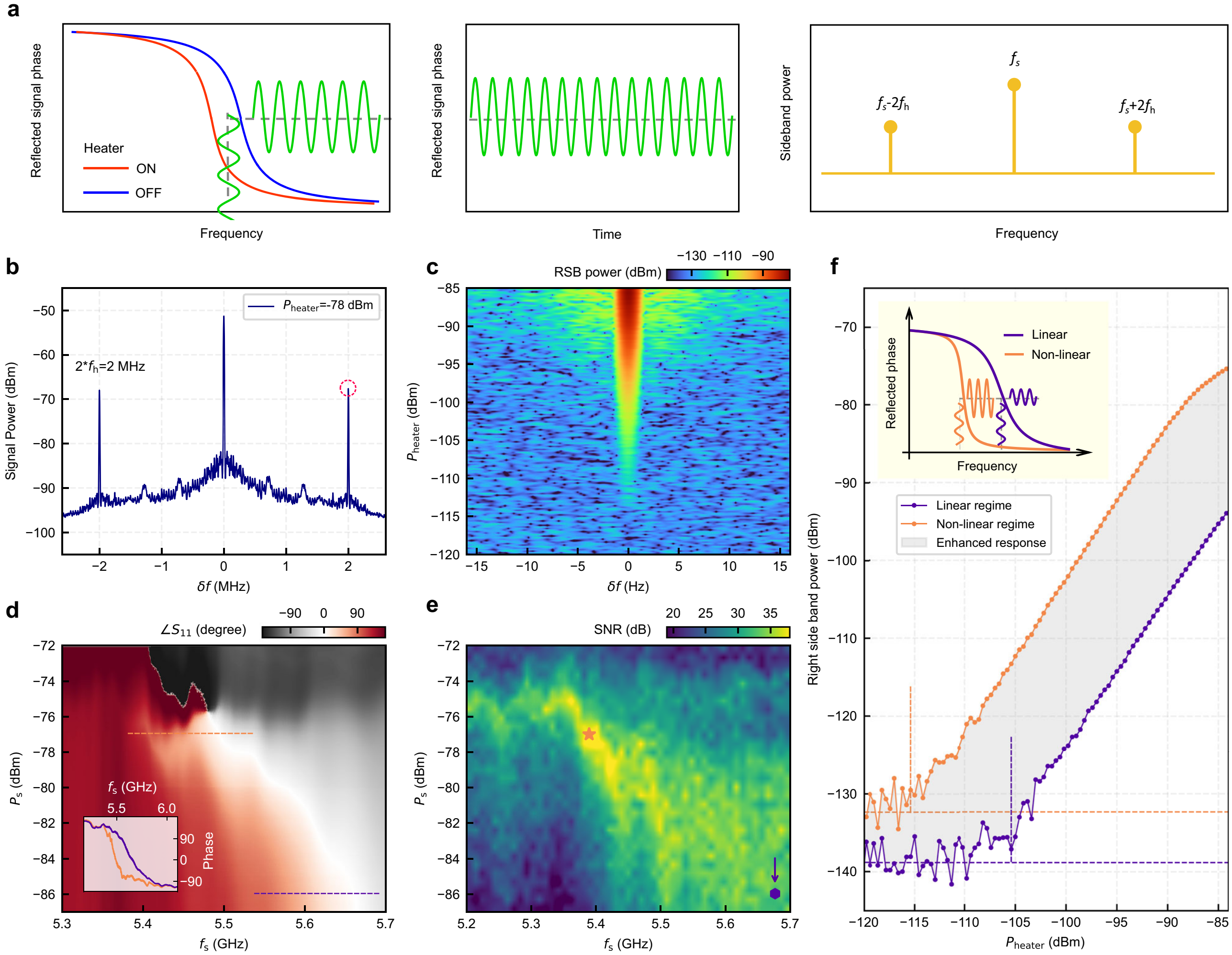

Fig. 3 | Graphene JPA as a sensitive bolometer. **a** Shows the sideband generation scheme. A modulated heater signal causes the phase ($\angle S_{11}$) at a certain frequency to oscillate over time, leading to the generation of sidebands in the frequency domain. The Joule heating effect of any modulated current at frequency f_h produces sidebands at $f_s \pm 2f_h$, where f_s is the pump signal frequency. **b** Shows a sideband spectrum of the bolometer device. The signal power is measured at the spectrum analyzer. Here we set the heater signal at $f_h = 1$ MHz, which causes the Joule heating in the device and hence modulation of the resonance at $2f_h$. Consequently, we see two sidebands around the pump signal at $f_s \pm 2f_h$. Here, δf is the detuned frequency from the pump signal set at $f_s = 5.47$ GHz. The V_g is set to 6 V and the heater power $P_{heater} = -78$ dBm. **c** Shows the right sideband (RSB) signal power measured as a function of heater power (P_{heater}) and detuned frequency (δf). Here we zoom in on the right sideband as shown by the red dashed circle in (**b**) and then resolve it as a function of P_{heater}. The x-axis δf is the detuned frequency from the right sideband in (**b**). As we increase the heater power, the sideband signal rises and eventually saturates. **d** Shows the non-linear phase diagram of the JPA, as a function of signal frequency (f_s) and power (P_s). The V_g is kept at 6 V, which fixes the linear resonance at low powers. With increasing signal power, the JPA becomes nonlinear, and the resonance starts to shift. An increase in power pushes the JPA towards a critical point beyond which any further increase in power makes it unstable (dark grey region). The inset shows the phase response at fixed powers marked by the purple and orange dashed horizontal lines on (**d**), in the low and high power regimes, respectively. **e** Shows the signal-to-noise ratio (SNR) map of the sideband signal measured as a function of pump signal frequency (f_s) and power (P_s). Here we keep the V_g at 6 V, set the $f_h = 1$ MHz, $P_{heater} = -95$ dBm, resolution bandwidth of the spectrum analyzer at 1 Hz, and measure the right sideband signal power at different points of the non-linear phase diagram of (**d**). We observe that when the JPA bolometer becomes non-linear, there is high SNR contrast in these regions. **f** Shows the sideband power plotted as a function of P_{heater} for linear and non-linear biasing of the bolometer at the points (linear: $f_s = 5.68$ GHz, $P_s = -97$ dBm) and (non-linear: $f_s = 5.39$ GHz, $P_s = -76.87$ dBm) respectively, marked by the purple hexagon and orange star in **e**. In the non-linear regime, the sideband signal is ~22 dB higher, and the sideband starts to rise in ~10 dB lower heater powers than that of the linear regime. This indicates that the device is more sensitive when operating in non-linear biasing. The inset schematic illustrates the phase sensitivity in the non-linear regime over the linear regime. The dashed horizontal lines indicate the noise floors.

diagram of the JPA. Next, at each point of this phase diagram, we bias the bolometer and measure its sideband response for the heater turned on and off. Eventually, we extract the signal-to-noise ratio (SNR) map of the bolometer across the non-linear phase diagram (see Supplementary Fig. 4b, c for details). Fig. 3e shows the SNR of the sideband signal measured as a function of the pump signal's frequency (f_s) and power (P_s). Here we keep the gate voltage fixed at $V_g = 6$ V, set the heater frequency at $f_h = 1$ MHz, and measure the right sideband signal power. In this measurement, the heater power is kept fixed at $P_{heater} = -95$ dBm for the ON state of the bolometer. We observe that when the bolometer becomes non-linear, there is a high SNR contrast in these regions. These high SNR regions are preferred for biasing the bolometer. See Supplementary Note 15 for the method used in optimizing the bias point of the bolometer for heat sensing. We note that the protocol used for biasing the bolometer through the SNR measurements does not require us to characterize the JPA gain profile, so we do not have this data for the current Device-1. The measured gain profile for Device-2 is shown in the Supplementary Fig. 17.

We next bias the device at linear and non-linear regimes to compare its bolometric sensitivity. Fig. 3f shows the sideband power plotted as a function of P_{heater} for linear and non-linear biasing of the bolometer at the biasing points (linear: $f_s = 5.68$ GHz, $P_s = -97$ dBm) and

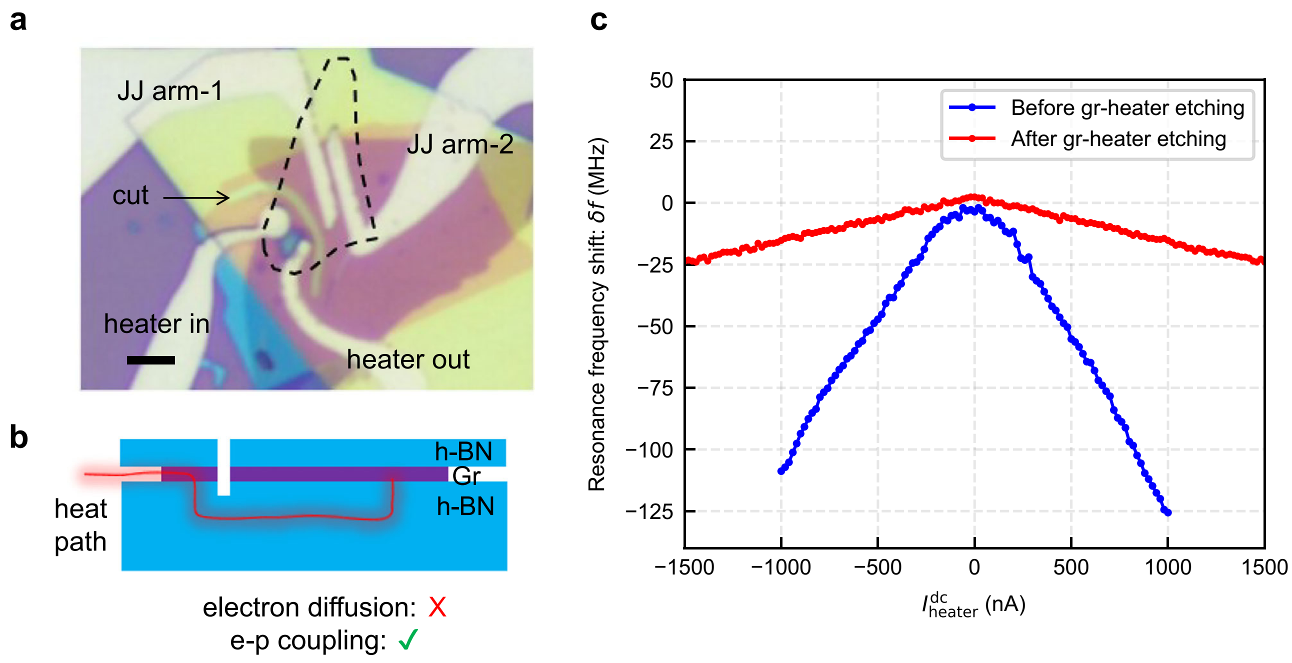

Fig. 4 | Heat conduction through phonon channels. a Shows an optical image of a control device (Device-4) for testing the heat conduction contribution of electrons and phonons. The JJ and the heater electrode share the same graphene flake marked by a dashed black line. After measuring one round of the device response, we etch the graphene heater to create a galvanic discontinuity between the heater and the JJ. The scale bar is 2 µm. **b** Shows the cross-sectional schematic of the hBN-gr-hBN stack. The white cut region shows the galvanic discontinuity for electron diffusion. We fully etch the top hBN, the graphene flake, and a little bit of bottom hBN (~5 nm) to ensure a full cut in graphene. In the heterostructure, the top hBN thickness is ~20 nm, and the bottom hBN thickness is ~60 nm. The only possible way for the heat to reach the JJ is through substrate phonons of hBN. **c** Shows resonance frequency shift as a function of DC Joule heating as described in Fig. 2a. After etching the graphene, the device still gets heated through the substrate phonons and shows a shift in the resonance frequency.

(non-linear: $f_s = 5.39$ GHz, $P_s = -76.87$ dBm), respectively. We find in the non-linear regime, the sideband signal is ~22 dB higher, and the signal starts to rise at ~10 dB lower heater powers than that of the linear regime. This indicates that the device is more sensitive when operating in non-linear biasing. We see around 6 dB increase in the noise floor in the non-linear regime, which is possibly set by the JPA gain and the system noise of the amplification chain. However, the SNR is now improved by 16 dB than that of the linear regime. The usage of a JPA helps us to enhance the bolometer response in two ways. First, in the non-linear regime, the device can sense smaller heat signals compared to the linear regime. This is due to the narrowing line width of the device (see Fig. 3d inset), which gives better sensitivity to the non-linear regime. Secondly, the JPA amplifies the upconverted sideband signals, as seen by the enhancement in the sideband power. This is a unique aspect of our integrated JPA bolometer device. Next, we extract the NEP of the device from the data shown in Fig. 3f, at the non-linear biasing. Supplementary Fig. 5 shows the extracted NEP of the bolometer. The best NEP value for $f_h = 1$ MHz is ~500 aW/$\sqrt{\mathrm{Hz}}$. In graphene bolometer devices, an open question in the field is the extent to which the injected heat couples to the JJ channel. We account for the fact that a finite fraction of the heat injected into the graphene heater leaks to the phonon bath before reaching the JJ. The heat transfer from the hot electrons of graphene to the hBN phonons is a surprising observation. We experimentally verify this heat transduction next.

Control experiment to study phononic heat transfer

There are two possible routes for the heat to reach the JJ – first, the hot electrons diffuse to the junction, and second, the phonons excited in the substrate carry heat to the JJ. To test the relative efficacy of these two channels we first study a device with a contiguous graphene connecting the heater and the JJ; subsequently, we sever the galvanic connection by etching the graphene in the same device—disconnecting the heater and JJ electrically. After severing the galvanic connection, we eliminate the channel of hot electrons perturbing the JJ response while still allowing for the phonons to affect the JJ. In our control experiment with an etched graphene heater device (see Fig. 4a, b), we observe that even after isolating the graphene heater and the JJ by introducing a cut in the graphene, heat can still propagate to the JJ via the phonons in the hBN. This phonon-mediated heat transfer causes a shift in the resonance frequency, as shown in Fig. 4c. This indicates that a finite portion of the heat injected into the device leaks to the substrate phonons. Notably, this response is seen despite interfacial Kapitza resistance at multiple interfaces. Studies utilizing scanning probes have demonstrated that hot electrons in graphene dissipate heat to atomic defects through resonant inelastic scattering for cooling[25,26]. However, such cooling processes at the device level, particularly in configurations involving small JJ channels, remain largely unexplored and challenging[27]. Here, our control experiment provides insights into heat dissipation to substrate phonons via atomic defects. Our finite element simulations estimate that approximately ~ 35% of the heat injected at the heater is lost to the phonon bath, as detailed in Supplementary Note 11.

Time constant measurements

Next, we measure the time constant of the bolometer experimentally. The response time of a bolometer quantifies the time required to excite and reset a bolometer. Using the graphene heater port, we heat the bolometer using short DC pulses sent in sequences while simultaneously probing its response with a pump signal at the resonance frequency of 4.848 GHz. The heater pulse width is set at 50 µs. We measure the digitized quadrature signal of the pump tone using a homodyne demodulation scheme (see Supplementary Note 6 for setup details). The quadrature signals (I, Q) are plotted as a function of time, see Fig. 5a. An exponential fit to the rising and falling edge yields the thermal time constants $\tau_{\mathrm{on}} = 4.45$ µs and $\tau_{\mathrm{off}} = 4.26$ µs. The data is

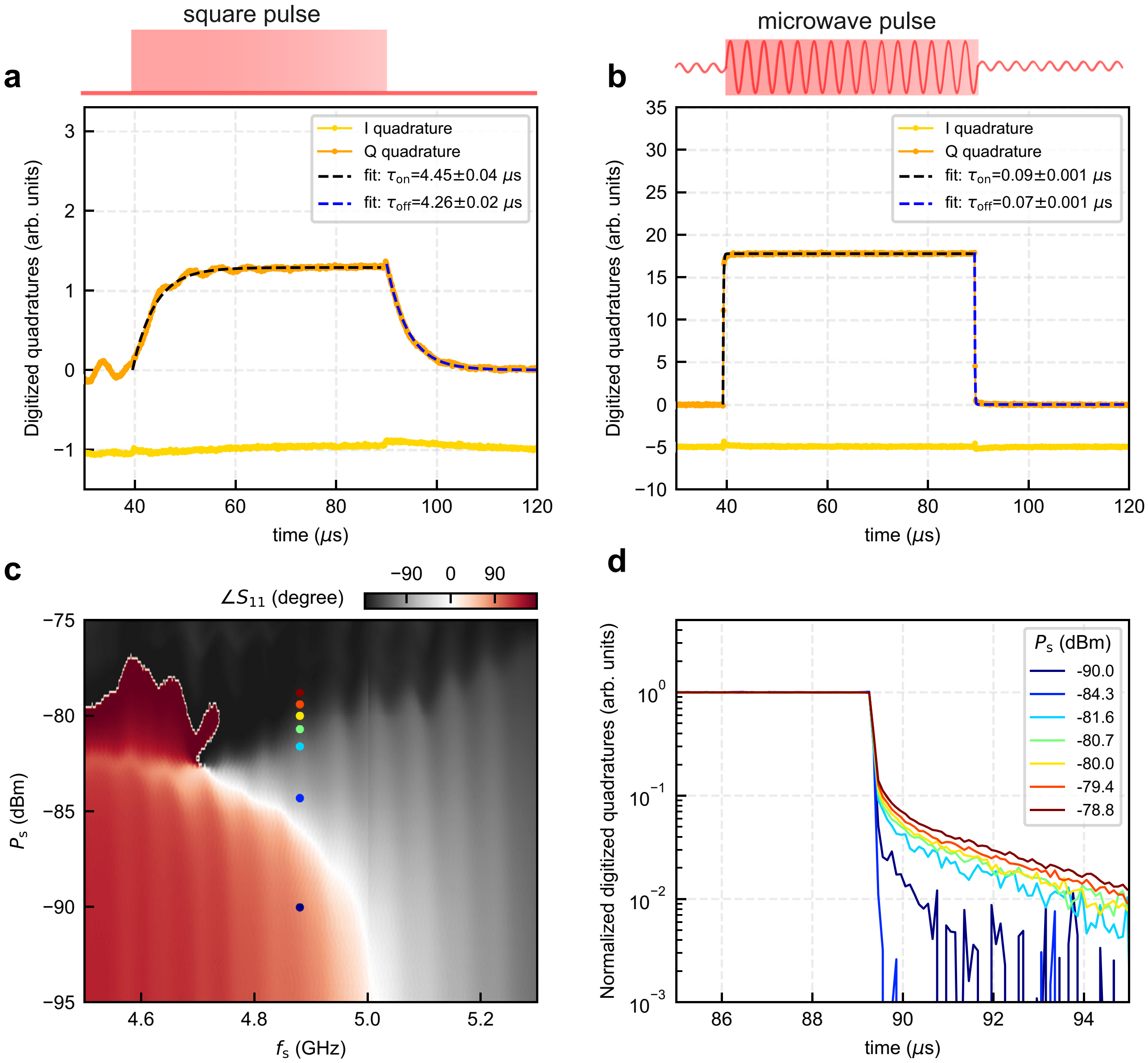

Fig. 5 | Time constants of the bolometer. a Shows the measured thermal time constant of the bolometer. We heat the bolometer using a short DC square pulse and simultaneously probe its response with a pump signal at 4.848 GHz in the linear biasing of the device. The heater pulse width is set at 50 μs. We measure the digitized quadrature signal of the pump tone using a homodyne demodulation scheme. The quadrature signals (I, Q) are plotted as a function of time. An exponential fit to the rising and falling edge yields the thermal time constants $\tau_{on} = 4.45\ \mu s$ and $\tau_{off} = 4.26\ \mu s$. **b** Shows the measured intrinsic time constant of the JPA. We probe the JPA using an amplitude-modulated microwave pulse, in the linear biasing of the device. The microwave pulse is made using a pump signal of 4.88 GHz mixed with a square pulse for amplitude modulation. The square pulse width is set at 50 μs. We measure the digitized quadrature signal of the pump pulse using a homodyne demodulation scheme. The quadrature signals (I, Q) are plotted as a function of time. An exponential fit to the rising and falling edge yields the intrinsic JPA time constants τ_{on} = 90 ns and τ_{off} = 70 ns. **c** Shows the non-linear phase diagram of the JPA plotted as a function of signal frequency (f_s) and power (P_s). The gate voltage is kept at $V_g = 2$ V. **d** Shows the measured intrinsic time constant of the JPA for different pump signal powers marked by colored dots in the non-linear phase diagram of (**c**). We probe the JPA using amplitude-modulated microwave pulses. We measure the digitized quadrature signal of the pump pulse using a homodyne demodulation scheme. The quadrature signals are plotted as a function of time. For small signal powers, the device responds fast; however, for large signal powers, the device becomes non-linear and eventually dissipative; hence, the response time lags and develops multiple time constants, evident from the slope change in the log scale.

taken at a fixed gate voltage and measured with averaging over multiple pulse sequences. Understanding the contributions of different heat-conducting channels is key to enhancing the time response of a thermal detector[28]. In our studies, we find that the rise and fall times are similar, about a few μs but varying across devices. See Supplementary Note 13 for the measured time constants on other devices.

The fact that there are sources for the transduction of hot electrons into phonons close to the JJ makes the defect-mediated phonons crucial in understanding the thermal response of our device. Past studies using the scanning probe technique show that there are atomic defects along the rough edges of the graphene sample, which contribute significantly to the transduction of hot electrons into phonons[25]. The path of electron diffusion into the JJ devices typically has a narrow entrance, through one open side (~300 nm) of the graphene segment. This could restrict the heating of the junction from electron diffusion. Hence, atomic defects along the rough edges of the 1D contacts, formed after etching graphene, could play an important role in the conversion of hot electrons into phonons, thereby heating the JJ. Similarly, for heat removal, the substrate phonons play a crucial role in thermalizing the graphene's electrons to the bath. Our understanding of the microscopic mechanism is qualitative at present and could explain the similarity of rise and fall times. Further studies are needed in the future to disentangle the effects of atomic defects on the interconversion of electrons into phonons and resulting thermal properties. One can fabricate vdW superconducting contacts (e.g, $NbSe_2$) to graphene without etching graphene to avoid defects and study their contributions further. In the Supplementary Note 16, we discuss the possible heat transfer mechanism in our device.

Next, to verify that the bolometer's time response is not constrained by the intrinsic time scale of the JPA, we measure the time response of the JPA. We drive the JPA with an amplitude-modulated microwave pulse and simultaneously probe it through the digitized quadrature signals using a homodyne demodulation scheme (see Supplementary Note 6 for setup details). During this experiment, the heater is not energized. At relatively low powers, the JPA exhibits a faster response with $\tau_{on} = 90$ ns and $\tau_{off} = 70$ ns, as shown in Fig. 5b. The response time of the JPA is limited by the intrinsic bandwidth of the device when operating close to the non-linear regime. Next, we vary the signal power of the microwave pulse to drive the JPA from the linear regime to the non-linear regime and eventually to the normal state of the JJ, following the probing points marked by the colored dots in Fig. 5c. In the linear regime, the JPA responds quickly, but as the power increases, the response slows down, as shown in Fig. 5d. This increase in response time at high power is expected in the non-linear regime of the JPA, where the internal bandwidth of the device decreases and also due to local heating at the JJ.

Discussion

In summary, we report the experimental realization of a bolometer device using a graphene JPA. The Kerr non-linearity of the JPA helps in enhancing the bolometer's sensitivity. When the bolometer is biased in the non-linear regime, it enhances the sideband signals (~100 times), resulting in an order of magnitude improvement in sensitivity compared to the linear regime. We achieve a best NEP ~ 500 $\mathrm{aW}/\sqrt{\mathrm{Hz}}$. We experimentally measure a fast thermal time constant of the bolometer of 4.26 μs. The sensitive and fast readout is a key feature of our device that will improve upon previous sensing schemes that relied on shifts in switching histograms to demonstrate exquisite sensitivity. Our device has the potential to sense single THz and NIR photons via a direct irradiation mechanism, where the graphene flake acts as a bus for carrying the hot electrons from the heated regions to the JJ, leading to a frequency shift in the device. The sensitivity of the bolometer can be improved further by using superconductors with a smaller energy gap, such as aluminum, for fabricating the JJs. Another approach could involve substrate engineering to enhance heat coupling to the JJ.

Our work extends the pathway for the exploration of 2D van der Waals materials-based devices for future-generation quantum sensors. Fast broadband bolometers have versatile applications in readout processes for cQED experiments[29,30], suggesting that our device could also be utilized for similar measurements. Recent experiments on MKIDs and SNSPDs have demonstrated significant pixel multiplexing capabilities in bolometer devices[13,31], which could also be adapted in large-scale graphene JPA bolometer devices for multiplexing applications. Furthermore, the nonlinear sensitivity enhancement, a critical feature unutilized in MKIDs and SNSPDs, is feasible within our device architecture while still enabling fast readout capabilities similar to those of MKIDs and SNSPDs.

Methods

The device fabrication process consists of a few steps. First, we pattern the coplanar waveguide (CPW) on SiO_2/Si substrate by standard e-beam lithography. The CPW is made of MoRe sputtered film of thickness 40 nm. Next, we make the MoRe-Al_2O_3-Al parallel plate capacitors (see Fig. 1b) by fixed-angle uniform rotation evaporation of Al_2O_3 and Al for thicknesses of 50 and 70 nm, respectively. Then, we prepare the hBN-graphene-hBN-graphite stack. We follow the scotch tape exfoliation of graphene and hBN crystals. A thick graphite flake is used for the bottom gate. We use PC (Poly(bisphenol A carbonate))/PDMS (polydimethylsiloxane) stamps for assembling the flakes. Once the stack is ready, we drop it on the CPW substrate. Next, we follow standard e-beam lithography for defining the JJ contacts on graphene. We etch the top hBN using CHF_3/O_2 reactive ion etching. Next, we do the MoRe sputtering to make the superconducting contacts of thickness 40 nm. Before deposition, we do an in-situ argon (Ar) plasma cleaning of the contacts. After sputtering, the resist lift-off is done in high-purity acetone. The device gets ready for characterization at this stage. Sometimes we face poor transparency of the contacts. In such cases, vacuum annealing at 350 °C in the forming gas environment helps to improve the transparency significantly.

Data availability

The experimental data used in the main text figures are available in Zenodo, with the identifier https://doi.org/10.5281/zenodo.15195742. Additional data related to this study are available from the corresponding authors upon request.

Code availability

The codes related to this study are available from the corresponding authors upon request.

References

1. Paolucci, F., Ligato, N., Germanese, G., Buccheri, V. & Giazotto, F. Fully superconducting Josephson bolometers for gigahertz astronomy. *Appl. Sci.* **11**, 746 (2021).
2. Braine, T. et al. Extended search for the invisible axion with the axion dark matter experiment. *Phys. Rev. Lett.* **124**, 101303 (2020).
3. De Visser, P. J., Baselmans, J. J. A., Bueno, J., Llombart, N. & Klapwijk, T. M. Fluctuations in the electron system of a superconductor exposed to a photon flux. *Nat. Commun.* **5**, 3130 (2014).
4. Pirro, S. & Mauskopf, P. Advances in bolometer technology for fundamental physics. *Annu. Rev. Nucl. Part. Sci.* **67**, 161–181 (2017).
5. Ikushima, K. et al. Photon-counting microscopy of terahertz radiation. *Appl. Phys. Lett.* **88**, 152110 (2006).
6. Inomata, K. et al. Single microwave-photon detector using an artificial λ-type three-level system. *Nat. Commun.* **7**, 12303 (2016).
7. Balembois, L. et al. Cyclically operated microwave single-photon counter with sensitivity of 10^{-22} W/Hz. *Phys. Rev. Appl.* **21**, 014043 (2024).
8. Yan, J. et al. Dual-gated bilayer graphene hot-electron bolometer. *Nat. Nanotechnol.* **7**, 472–478 (2012).
9. Efetov, D. K. et al. Fast thermal relaxation in cavity-coupled graphene bolometers with a Johnson noise read-out. *Nat. Nanotechnol.* **13**, 797–801 (2018).
10. Lee, G.-H. et al. Graphene-based Josephson junction microwave bolometer. *Nature* **586**, 42–46 (2020).
11. Kokkoniemi, R. et al. Bolometer operating at the threshold for circuit quantum electrodynamics. *Nature* **586**, 47–51 (2020).
12. Walsh, E. D. et al. Josephson junction infrared single-photon detector. *Science* **372**, 409–412 (2021).
13. Oripov, B. G. et al. A superconducting nanowire single-photon camera with 400,000 pixels. *Nature* **622**, 730–734 (2023).
14. Cai, X. et al. Sensitive room-temperature terahertz detection via the photothermoelectric effect in graphene. *Nat. Nanotechnol.* **9**, 814–819 (2014).
15. El Fatimy, A. et al. Epitaxial graphene quantum dots for high-performance terahertz bolometers. *Nat. Nanotechnol.* **11**, 335–338 (2016).

16. Tielrooij, K. J. et al. Photoexcitation cascade and multiple hot-carrier generation in graphene. *Nat. Phys.* **9**, 248–252 (2013).
17. Brida, D. et al. Ultrafast collinear scattering and carrier multiplication in graphene. *Nat. Commun.* **4**, 1987 (2013).
18. Walsh, E. D. et al. Graphene-based Josephson-junction single-photon detector. *Phys. Rev. Appl.* **8**, 024022 (2017).
19. Katti, R. et al. Hot carrier thermalization and Josephson inductance thermometry in a graphene-based microwave circuit. *Nano Lett.* **23**, 4136–4141 (2023).
20. Huang, B. et al. Graphene calorimetric single-photon detector. Preprint at http://arxiv.org/abs/2410.22433 (2024).
21. Aumentado, J. Superconducting parametric amplifiers: the state of the art in Josephson parametric amplifiers. *IEEE Microw. Mag.* **21**, 45–59 (2020).
22. Hatridge, M., Vijay, R., Slichter, D. H., Clarke, J. & Siddiqi, I. Dispersive magnetometry with a quantum limited SQUID parametric amplifier. *Phys. Rev. B* **83**, 134501 (2011).
23. Sarkar, J. et al. Quantum-noise-limited microwave amplification using a graphene Josephson junction. *Nat. Nanotechnol.* **17**, 1147–1152 (2022).
24. Butseraen, G. et al. A gate-tunable graphene Josephson parametric amplifier. *Nat. Nanotechnol.* **17**, 1153–1158 (2022).
25. Halbertal, D. et al. Imaging resonant dissipation from individual atomic defects in graphene. *Science* **358**, 1303–1306 (2017).
26. Kong, J. F., Levitov, L., Halbertal, D. & Zeldov, E. Resonant electron-lattice cooling in graphene. *Phys. Rev. B* **97**, 245416 (2018).
27. Fried, C. et al. Performance limits due to thermal transport in graphene single-photon bolometers. *Phys. Rev. Appl.* **21**, 014006 (2024).
28. Gasparinetti, S. et al. Fast electron thermometry for ultrasensitive calorimetric detection. *Phys. Rev. Appl.* **3**, 014007 (2015).
29. Opremcak, A. et al. Measurement of a superconducting qubit with a microwave photon counter. *Science* **361**, 1239–1242 (2018).
30. Gunyhó, A. M. et al. Single-shot readout of a superconducting qubit using a thermal detector. *Nat. Electron.* **7**, 288–298 (2024).
31. Walter, A. B. et al. The MKID Exoplanet Camera for Subaru SCExAO. *Publ. Astronom. Soc. Pac.* **132**, 125005 (2020).

Acknowledgements

We thank Vibhor Singh, Eli Zeldov, Vishal Ranjan, and R. Vijay for their helpful discussions and comments. We thank Kishor V. Salunkhe, Gaurav Bothara, Ritajit Kundu, Mahesh Hingankar, and Digambar A. Jangade for useful discussions and experimental assistance. This material is based upon work supported by the Air Force Office of Scientific Research under award number FA2386-23-1-4031. We acknowledge the Nanomission grant SR/NM/NS-45/2016 and DST SUPRA SPR/2019/001247 grant along with the Department of Atomic Energy of Government of India 12-R&D-TFR-5.10-0100 for support. Preparation of hBN single crystals is supported by the Elemental Strategy Initiative conducted by the MEXT, Japan (Grant Number JPMXP0112101001) and JSPS KAKENHI (Grant Numbers 19H05790 and JP20H00354).

Author contributions

J.S. fabricated the devices, led the measurements, and analyzed the data. K.M. and P.S. helped with measurements and analysis. A.S., H.A., and P.S. assisted in the device fabrication. R.R. and A.S. assisted in the finite element simulations. A.B. assisted in the time constant measurements. M.P.P. assisted in microwave PCB fabrications. K.W. and T.T. grew the hBN crystals. J.S. and M.M.D. wrote the manuscript with input from everyone. M.M.D. supervised the project.

Funding

Open access funding provided by Department of Atomic Energy.

Competing interests

The authors declare no competing interests.

Additional information

Supplementary information The online version contains supplementary material available at https://doi.org/10.1038/s41467-025-62480-9.

Correspondence and requests for materials should be addressed to Joydip Sarkar or Mandar M. Deshmukh.

Peer review information *Nature Communications* thanks the anonymous reviewers for their contribution to the peer review of this work. A peer review file is available.